Mass independent fractionation of even and odd mercury isotopes during free tropospheric mercury oxidation

Xuewu Fu[1,2], Martin Jiskra[1,3], Xu Yang[1,2], Nicolas Marusczak[1], Maxime Enrico[1,$], Jerome Chemleff[1], Lars-Eric Heimbürger[1,%] François Gheusi[4], Jeroen E. Sonke[1,*]

[1] Géosciences Environnement Toulouse, CNRS/IRD/CNRS/Université de Toulouse, France

[2] State Key Laboratory of Environmental Geochemistry, Institute of Geochemistry, Chinese Academy of Sciences, Guiyang, 550081, China.

[3] Environmental Geosciences, University of Basel, Switzerland

[4] Laboratoire d'Aérologie, CNRS/IRD/Université de Toulouse, France

[$] present address: Harvard John A. Paulson School of Engineering & Applied Sciences, Harvard University, Cambridge, MA, USA

[%] present address: Mediterranean Institute of Oceanography, Aix Marseille Université, CNRS/IRD, Université de Toulon, IRD, Marseille, France

* Corresponding Author: jeroen.sonke@get.omp.eu

Abstract. Even mercury (Hg) isotope mass independent fractionation (MIF), observed in rainfall globally, is used to quantify atmospheric Hg deposition pathways. The underlying reaction and MIF mechanism are unknown however. Here we investigate the Hg isotope composition of free tropospheric gaseous elemental Hg^0 and Hg^{II} forms. We find that gaseous oxidized Hg^{II} has positive $\Delta^{199}Hg$, $\Delta^{201}Hg$, $\Delta^{200}Hg$, and negative $\Delta^{204}Hg$ signature, similar to rainfall Hg^{II}, and we document rainfall Hg^{II} $\Delta^{196}Hg$ to be near-zero. Cloud water and rainfall Hg^{II} show enhanced odd MIF compared to gaseous Hg^{II}, indicating in-cloud Hg^{II} photoreduction. Hg MIF observations of free tropospheric Hg^0 dynamics show how net Hg^0 oxidation leads to opposite MIF in Hg^0 and Hg^{II}. A $\Delta^{200}Hg$ mass balance for Hg^0 and Hg^{II} forms suggests that measurements and models underestimate the tropospheric Hg^{II} pool.

Introduction

Modern anthropogenic Hg emissions (2400 Mg a^{-1}) outweigh natural Hg emissions by an order of magnitude (Bagnato et al., 2014; Streets et al., 2019). Hg emissions are mostly in the form of gaseous elemental Hg (GEM), which has a long atmospheric life-time against oxidation to divalent reactive Hg (RM) forms that include gaseous oxidized Hg (GOM) and particulate bound Hg (PBM) (Amos et al., 2012). RM is rapidly deposited to continental and marine ecosystems where microbial activity transforms inorganic Hg into the bioaccumulating and toxic methylmercury form (Fitzgerald and Lamborg, 2004). Predicting the impact of anthropogenic Hg emission scenarios on global Hg deposition requires detailed understanding of atmospheric Hg transformations and of GEM oxidation in particular. Two decades of atmospheric Hg research using mountain-top and in-flight observations, experimental and theoretical reaction kinetics, and coupled 3D atmosphere-ocean chemistry and transport models, have given broad understanding of atmospheric Hg dynamics (Ariya et al., 2015; Dibble et al., 2020; Donohoue et al., 2006; Holmes et al., 2010; Seigneur et al., 2004). Experimental, theoretical and modeling studies suggest Hg oxidation initiated by bromine (Br) radicals to be faster than by ozone or OH (Horowitz et al., 2017; Wang et al., 2014), yet major uncertainties in RM concentrations, oxidation and reduction mechanisms and rates remain (Jaffe et al., 2014; Saiz-Lopez et al., 2018; Weiss-Penzias et al., 2015).

Hg stable isotope analysis of atmospheric Hg compounds may provide new information on Hg emission sources and complex atmospheric redox cycling. During the last decade, significant advances have been made in the measurement of Hg isotope compositions of biogeochemical reservoirs (Kwon et al., 2020). Laboratory and field evidence suggests that processes controlling Hg emission such as reduction/oxidation, adsorption/desorption, or volatilization can induce significant mass dependent Hg isotope fractionation (MDF,

57 δ^{202}Hg signature)(Jiskra et al., 2015; Kritee et al., 2012; Wiederhold et al., 2010). Large mass independent Hg
58 isotope fractionation (MIF) of odd Hg isotopes by the magnetic isotope effect has been observed in aqueous
59 photochemical Hg reduction experiments (Δ^{199}Hg, Δ^{201}Hg signatures) (Bergquist and Blum, 2007; Zheng and
60 Hintelmann, 2009). Odd-MIF signatures imparted on inorganic Hg and methyl-Hg by photochemistry can be
61 traced into all Earth surface environments, i.e sediments, biota, atmosphere, soils etc. Unusual even isotope MIF
62 (Δ^{200}Hg, Δ^{204}Hg) has been observed in rainfall and snowfall globally (Chen et al., 2012; Demers et al., 2013;
63 Gratz et al., 2010), and has been speculated to originate in GEM photo-oxidation at and above the tropopause
64 (Chen et al., 2012). The exact even-MIF mechanism and even-MIF inducing Hg transformation(s) remain
65 essentially unknown.

66 In this study we investigate Hg isotope composition of GEM, RM, and cloud water at the high altitude Pic
67 du Midi Observatory (PDM, 2877m, France). The PDM regularly receives free tropospheric air masses that are
68 enriched in RM and depleted in GEM (Fu et al., 2016a). High frequency, 12h and 24h GEM isotope observations
69 of a free tropospheric air mass rich in GOM and depleted in GEM are investigated to derive MDF and MIF
70 factors for net oxidation. Photoreduction experiments on rainfall are made to constrain atmospheric aqueous
71 MDF and MIF factors. Finally, we investigated the even-MIF on the low abundance ^{196}Hg isotope to help
72 understand potential even-MIF mechanisms.
73

74 **Materials and methods**

75 **Site description and ancillary parameters**

76 The Pic du Midi Observatory (PDM, 0.14º E, 42.94º N, 2877 m a.s.l) is a high-altitude monitoring station
77 situated on top of an isolated peak on the north edge of the central Pyrenees Mountains, Southwest France. The
78 PDM receives free tropospheric air from the Northeast Atlantic Ocean and Europe and boundary layer air from
79 upslope winds in Spain and southwest France (Gheusi et al., 2011; Hulin et al., 2019). The station receives
80 predominantly southerly and southwesterly winds (> 70 %) across the main range of Pyrenees (Hulin et al.,
81 2019). There are no major anthropogenic Hg emission point sources around the station or in the surrounding
82 areas.
83

84 **Atmospheric sampling and processing**

85 Short-term (12/24h) variations in atmospheric GEM isotopic composition were investigated from 19 to 28 in
86 Dec 2012 at PDM using large chlorine-impregnated activated carbon (CLC) traps. Traps with 600 mg CLC were

utilized for 24 hour sampling at a flow rate of ~ 10 L min^{-1}; whereas traps with 1000 mg of CLC were utilized for 12 hour sampling at a flow rate of ~ 20 LPM (Fu et al., 2014). The sampling inlets of the CLC traps (heated at 70ºC to avoid water condensation), preceded by a pre-burned 47mm quartz fiber filter were connected to a Tekran 1104 Teflon coated sampling manifold, operating at 100 LPM and 70ºC, and installed into the prevailing wind direction. Sampling flow rates of CLC traps were regulated via ball flow meters installed at the outlets of the vacuum pumps, and the total sampling volumes of the traps were recorded using gas meters. Similar to Arctic studies (Berg et al., 2013; Steffen et al., 2005) we find that the Hg collected on CLC traps reflects the GEM fraction, and is not confounded by the GOM fraction. Both GOM and PBM fractions are retained on the quartz filter preceding the CLC trap. Quartz has been previously shown to efficiently scavenge GOM over time periods shorter than 24h (Lyman and Jaffe, 2011; Lynam and Keeler, 2002). CLC traps were thermally decomposed (25ºC to 1000ºC over 8h) in a Hg-free oxygen flow (25 ml min^{-1}) in a tube furnace. Combustion products were further decomposed in a 2nd pyrolizer tube furnace at 1000°C, and purged into a 10 ml 40 vol% $2HNO_3$/1HCl oxidizing solution (Sun et al., 2013). CLC sampling efficiencies were better than 95%, mean recovery efficiencies were 87%, and full procedural blanks <2% of Hg concentrations in trapping solutions (Fu et al., 2014).

Twelve samples of the atmospheric RM (RM=GOM+PBM) were obtained using Millipore polyethersulfone cation exchange membranes (CEMs, Millipore, 0.45 µm pore size, 47 mm and 90 mm diameter (Marusczak et al., 2017)) at the PDM from June to October 2014, with sampled air volumes between 25 and 77 m^3. Cloud water samples were collected from July to November 2014 with a CASCC-2 sampler at the PDM (Demoz et al., 1996). Rainfall was sampled from July to August 2014 150km downwind from the PDM at 800m altitude in the Pyrenees foothills using acid-washed polypropylene buckets and reported elsewhere (Enrico et al., 2016). Snowfall and rainfall was collected at the PDM and the Geosciences Environnement Toulouse (GET, Toulouse, France, 43.54º N, 1.48º E) laboratory between 2016 and 2017 using the same methods. Cloud water, rainfall and snowfall samples collected after each event were transferred into pre-cleaned Pyrex glass bottles (1 and 2 L volume), then oxidized by adding 0.1 – 1 % BrCl, and kept refrigerated before Hg concentration analysis by CVAFS and further pre-concentration for Hg isotope analysis. Hg from rain and cloud water samples was pre-concentrated by reducing and purging Hg with $SnCl_2$ and a clean argon flow and subsequent trapping in an oxidizing solution, following Sherman, et al. (Sherman et al., 2012). Recoveries of procedural standards, rainfall and cloud water samples was >95%. RM on CEMs was leached in 20 vol% $2HNO_3$/1HCl with blanks <4% of sampled RM.

Hg isotope fractionation factors during aqueous photochemical reduction of rainwater was studied using a solar simulator (see (Yang et al., 2019) for details). A low Hg level (2.6 ng L^{-1}) rainfall sample 'GET rain 4' obtained at GET was spiked with 103 ng L^{-1} NIST 3133 and equilibrated for 48 in the dark. A 450 mL aliquot was then transferred into an acid-cleaned quartz reactor, and illuminated for 24h with the solar spectrum from a Xe lamp. After 24, the 78 ng L^{-1} dissolved Hg(II) remaining in the 450mL reactor volume was transferred to a pre-cleaned 1L Pyrex bottle, and pre-concentrated for Hg isotope analysis.

Mercury isotopic analysis

Hg isotope ratios were measured using cold vapor multi-collector inductively coupled plasma mass spectrometry (CV-MC-ICPMS, Thermo-Finnigan Neptune, and Neptune Plus) at the Midi-Pyrenees Observatory, Toulouse, France following the methods described in previous studies (Jiskra et al., 2019; Obrist et al., 2017). Instrumental mass bias of MC-ICPMS was corrected by standard-sample-standard bracketing using NIST3133 Hg at matching concentrations. Hg isotopic composition is reported in delta notation (δ) in units of per mil (‰) referenced to the bracketed NIST 3133 Hg standard (Blum and Bergquist, 2007): $\delta^{xxx}Hg = [(^{xxx}Hg/^{198}Hg)_{sample}/(^{xxx}Hg/^{198}Hg)_{NIST3133} -1]$, where xxx represent Hg isotope masses 199, 200, 201, 202, 204. MIF values are expressed by "capital delta (Δ)" notation (‰), which is the difference between the measured values of $\delta^{199}Hg$, $\delta^{200}Hg$, $\delta^{201}Hg$ and those predicted from $\delta^{202}Hg$ using the kinetic MDF law: $\Delta^{xxx}Hg$ (‰) = $\delta^{xxx}Hg - (\beta^{xxx} \times \delta^{202}Hg)$, where β^{xxx} is -0.5074, 0.2520, 0.5024, 0.7520, 1.493 for the 196, 199, 200, 201, and 204 Hg isotopes respectively. The analytical uncertainty of isotopic analysis was assessed by repeated analysis of the UM-Almaden and ETH-Fluka standards over different analysis sessions and at Hg concentrations corresponding to the samples. The overall mean values of $\delta^{202}Hg$, $\Delta^{199}Hg$, $\Delta^{200}Hg$, $\Delta^{201}Hg$, and $\Delta^{204}Hg$ for all the UM-Almaden standards in the 0.5 to 1.5 ng g^{-1} range were -0.56 ± 0.07 ‰, -0.04 ± 0.08 ‰, -0.01 ± 0.09 ‰ and -0.05 ± 0.09 ‰, and 0.04 ± 0.19 ‰ (2SD, n = 11) respectively, which agree well with previously reported values (Blum and Bergquist, 2007). The procedural standard for rainfall pre-concentration, i.e. rainfall sample 'GET rain 4' spiked with 103 ng g^{-1} NIST 3133 showed good recovery and no isotopic bias (Supporting Data). In the present study, the analytical uncertainty of CV-MC-ICPMS isotope analysis of RM, GEM, rainfall, and snowfall is the 2SD uncertainty of the UM-Almaden standard, unless the 2SD uncertainty on repeated analysis of the same sample over different analytical sessions was larger.

To attempt rainfall $\Delta^{196}Hg$ analysis, we screened rainfall samples obtained at GET in 2016 for both high Hg concentration levels and high volume single events. Rainfall sample 'GET rain 6' was the only sample

147 retained as it consisted of a single thunderstorm event of 20.5 L, collected in the 8 large buckets, and had a Hg
148 concentration of 6.0 ng L^{-1}. The entire 20.5L volume was pre-concentrated 1200x in a single large Pyrex glass
149 bottle to a final concentration of 8.0 ng g^{-1} in 15.3 g of 20vol% iAR. The sample was run in duplicate during
150 two different days using dedicated UM-Almaden and ETH-Fluka standards, also at 8.0 ng g^{-1}. All individual
151 sample and standard results are given in the Supporting Data. The signals obtained on the ^{196}Hg and ^{202}Hg
152 isotopes during these sessions were 15mV and 3 Volt. We recommend the use of 10^{12} or 10^{13} Ω resistors on the
153 signal amplifier of the ^{196}Hg Faraday cup. The 2σ uncertainty, based on sample, UM-Almaden, and ETH-Fluka
154 replicates, on $\Delta^{196}Hg$ during these analysis sessions were 0.19‰ (Supplementary Data).
155
156 **Ancillary parameters**
157 Atmospheric Hg speciation at the PDM, including GEM, GOM and PBM, was continuously measured off
158 the same sampling manifold with a Tekran 2537/1130/1135 system (Tekran Inc., Canada) (Fu et al., 2016a;
159 Marusczak et al., 2017). Automated GOM and PBM analyses are subject to mounting criticism as the techniques
160 lack calibration, collection efficiency control and interference correction (Jaffe et al., 2014). We partly address
161 these issues by parallel manual sampling of RM (GOM + PBM) on CEMs (Huang et al., 2013). We find that
162 denuder-based GOM at the PDM is systematically underestimated by a factor of 1.56 for which we correct
163 (indicated by an asterisk hereafter, i.e. GOM*)(Marusczak et al., 2017). Atmospheric CO and O_3 concentrations
164 were continuously measured using a TEI (Thermo Environmental Instruments Inc. USA) 48CTL gas filter
165 correlation analyzer and 49C UV-absorption ozone analyzer, respectively, following published procedures
166 (Gheusi et al., 2011). Meteorology, CO and O3 data at the PDM were provided through the Pyrenean platform
167 for observation of the atmosphere (P2OA, http://p2oa.aero.obs-mip.fr).
168
169 **Air mass backward trajectories**
170 Seven day backward trajectories ending at PDM at a height of 3000 m above sea level were calculated
171 every 2 hours with simulated gridded meteorological data from the Weather Research and Forecasting (WRF)
172 model Version 3.4 with the Noah Land Surface Model, Thompson microphysics scheme, Grell-3 cumulus
173 scheme, Dudhia radiation physics scheme, YSU scheme for PBL. The modeled domain of meteorological data
174 mainly covered the eastern North Atlantic Ocean and European area, with a time resolution of 1 h, 400 × 800
175 grid cells at a 12-km horizontal resolution, and vertical levels of 50 from 1000 hPa to 20 hPa. All the trajectories
176 during the 12h, 24h of individual Hg isotope samples were grouped into an average backward trajectory to show

the mean air mass source region of samples.

Results and discussion

GEM isotope compositions

The nine day sampling period from 19 to 28 Dec 2012 was characterized by a shift from cloudy conditions (days 1-2, samples D1-D3) to clear skies (days 3-5, samples D4-D9), and back to clouds (days 7-9, samples D10-D14). The wind direction was predominantly southwest bringing North-Atlantic Ocean air masses, over northwest Spain, to the PDM. The continuous Hg speciation observations show a pronounced increase in GOM* to 252 pg m^{-3} (48h mean), and concurrent decrease in GEM during samples D4-D6 (clear skies, Figure 1, Table S1). Back trajectory analysis, and low observed relative humidity and CO, suggest that the high GOM event represents the intrusion of a free tropospheric air mass that originated at 5000m (550hPa, Figures 1, 2). Such intrusions are typical at PDM, e.g. 61 events were registered over a one year period from Nov 2011 to Nov 2012 (Fu et al., 2016a). The intrusions are of particular interest as they offer a snapshot of the free troposphere where GEM oxidation is thought to take place (Fu et al., 2016a; Lyman and Jaffe, 2011; Swartzendruber et al., 2006; Timonen et al., 2013). δ^{202}Hg, Δ^{199}Hg and Δ^{200}Hg of 12h and 24h GEM samples collected from 19 to 28 Dec 2012 were in the range of 0.16 to 0.51‰ (δ^{202}Hg, mean = 0.34‰), -0.31 to -0.11‰ (Δ^{199}Hg, mean = -0.23‰), and -0.17 to 0.04‰ (Δ^{200}Hg, mean = -0.07‰) (Table S1). These observations are consistent with a single two-week integrated GEM isotope sample B19, collected over the same period 19 to 28 Dec 2012 at a lower flow rate of 2 L min^{-1}. with δ^{202}Hg of 0.39‰, Δ^{199}Hg of -0.27‰, Δ^{200}Hg of -0.10 ‰ (Fu et al., 2016b).

RM, cloud water and rainfall Hg isotope compositions

In a previous study we found that rainfall Hg isotope signatures 150km east from the PDM are typical of rainfall observations globally, with a mean δ^{202}Hg 0.17 ± 0.33 ‰ and significantly positive odd MIF (Δ^{199}Hg = 0.72 ± 0.15 ‰; Δ^{201}Hg = 0.76 ± 0.14 ‰) and even-MIF (Δ^{200}Hg = 0.21 ± 0.04 ‰; Δ^{204}Hg = -0.33 ± 0.10 ‰, all 1σ, n = 9) (Figure 3, Table S1, Enrico et al., 2016). Here we find that PDM cloud water THg concentrations and MDF and MIF signatures are not significantly different from PDM and regional rainfall (p=0.26 to 0.79). For the first time we observe that RM, i.e. GOM+PBM, at PDM also has positive odd MIF (Δ^{199}Hg = 0.44 ± 0.17 ‰; Δ^{201}Hg = 0.44 ± 0.10 ‰) and even-MIF (Δ^{200}Hg = 0.15 ± 0.06 ‰; Δ^{204}Hg = -0.22 ± 0.17 ‰, all 1σ, n = 12), similar to PDM cloud water and rainfall (Figure 3) and similar to global rainfall (Δ^{199}Hg = 0.35 ± 0.19 ‰; Δ^{200}Hg = 0.14 ± 0.06 ‰; Δ^{201}Hg = 0.35 ± 0.20 ‰ (Kwon et al., 2020). Demers et al. (2013) were the first to point out a negative

correlation between Δ^{200}Hg and Δ^{204}Hg in rainfall (Demers et al., 2013). Our work at the PDM extends this relationship to RM, cloud water, and GEM phases (Figure 3). The presence of even- and odd-MIF in RM suggests that globally observed Hg MIF signatures in rainfall are inherited from RM. Equally important, the isotopic composition of RM is in stark contrast with that of GEM (Figure 3), even though the only transformation that separates the two forms of Hg is net oxidation. This corroborates the suggestion that net photochemical oxidation of GEM is responsible for even MIF (Chen et al., 2012), but it does not identify the oxidative or reductive nature of the MIF inducing step among the myriad of possible reactions that drive atmospheric net GEM oxidation.

Cloud water and rainfall δ^{202}Hg (0.17 ± 0.34 ‰) and Δ^{199}Hg (0.21 ± 0.04 ‰) show significant enrichment in the heavier and in the odd Hg isotopes relative to mean RM δ^{202}Hg (-0.73 ± 0.63 ‰) and Δ^{199}Hg (0.44 ± 0.18 ‰)(both $p<0.001$, all mean, 1σ). We investigated if this is caused by in-cloud Hg^{II} photoreduction, by incubating a rainfall sample spiked with 103 ng L^{-1} of NIST 3133 Hg. After 24h exposure to artificial sunlight from a Xe lamp, the Hg concentration had dropped to 78 ng L^{-1} and small positive shifts in δ^{202}Hg (0.15 ‰), Δ^{199}Hg (0.10‰), and Δ^{201}Hg (0.11‰), but not Δ^{200}Hg (-0.03‰) were detected. These observations are consistent with limited, slow in-cloud Hg^{II} photoreduction affecting cloud water and rainfall MDF and odd-MIF. Finally, we observe for the first time the Δ^{196}Hg signature to be near-zero (-0.06 ± 0.19‰, 2σ, n=2) in the 'GET rain 6' sample (Figure 4), which has pronounced Δ^{199}Hg (0.70‰), Δ^{200}Hg (0.25‰), Δ^{201}Hg (0.82‰), and Δ^{204}Hg (-0.45‰). The observation that the least abundant ^{196}Hg, and most abundant ^{202}Hg isotope, both referenced to ^{198}Hg, show near-zero MIF, further suggests that nuclear self-shielding is unlikely to be the mechanism responsible for atmospheric Hg MIF.

δ^{202}Hg and Δ^{199}Hg variation during the high GOM event

We obtained additional evidence for odd and even MIF during net GEM oxidation from the high frequency (12-24h) GEM isotope observations during the free tropospheric air mass intrusion, enriched in GOM and depleted in GEM (Figure 1, days 4-6). The high GOM event showed GOM* concentrations of 252 pg m^{-3} from 23-24 Dec (48h mean). The GOM event was accompanied by low CO concentrations, depleted GEM concentrations, and low relative humidity (Figure 1,2), which is consistent with previous studies and indicative of GOM production by oxidation of GEM in a free tropospheric air mass (Gratz et al., 2015; Shah et al., 2016). Seven-day back-trajectories of the GOM event and of the pre- (days 1-3) and post-event (days 7-9) air masses illustrate the important control of cloudiness along the trajectory on detected GOM levels at the PDM (Figure 2). Pre/post-

GOM-event air masses generally travelled at 700-1000 hPa (3000m – 0m asl) over the N-Atlantic Ocean (35-50ºN) with RH from 60-100% and daytime solar radiation <200 w m^{-2} suggestive of GOM scavenging by clouds (Figure 1,2). GOM-event air masses also travelled over the subtropical N-Atlantic Ocean, though at lower latitudes (20-35ºN), and higher altitudes of 500-900 hPa (5500m – 1500m asl) with RH from 0-40% and daytime solar radiation from 200-500 w m^{-2} suggestive of clear skies. GOM-event mean ozone (47 ± 2 ppbv, sd), CO (83 ± 3 ppbv, sd) and relative humidity (34 ± 10%, sd) are typical of lower to middle free tropospheric air. Both the back trajectories and ozone, CO, RH characteristics suggest a negligible influence of stratospheric air on the observed GOM-event.

A negative correlation between GEM and GOM* was observed during the 8-day study period of Dec 2012 with GOM*/GEM slope of -0.44 ± 0.10 (r^2 = 0.66; Figure 5). It has been previously suggested that GOM/GEM slopes higher than -1 reflect the loss of newly produced GOM by scavenging processes, or the mixing with other air masses with different GEM levels (Lyman and Jaffe, 2011; Swartzendruber et al., 2006). PBM concentrations during the high-GOM event are uniformly low (mean, 4 pg m^{-3}) and RH and solar radiation levels along the back trajectories do not support an important scavenging sink (Figure 2). A prerequisite for the GOM*/GEM slope analysis is that the ensemble of observations has a common air mass origin, which is not the case here. The back trajectory analysis of our 8-day observations suggests overlapping altitudes for pre- and post-event (3000m – 0m asl) and GOM-event (5500m – 1500m asl) air masses. Published reviews of GEM altitude profiles suggest little variation up to 5km (Holmes et al., 2010). However, observed and modeled boundary layer GEM levels suggest maximum levels between 30-60ºN, corresponding to mid-latitude emission sources, and declining levels from 30ºN to the equator (1% decrease in GEM per degree latitude, Holmes et al., 2010). As mentioned above pre/post-event and GOM-event back trajectories point out different latitudinal origins of 20-35ºN and 35-50ºN respectively. It seems therefore plausible that the original GEM levels in pre/post-event and GOM-event levels air masses were different due to different latitudinal air mass origins. A correction for latitudinal confounding allows estimating original GEM levels to be 15% lower in the GOM-event air masses, based on the 1% drop in GEM per degree latitude, and yields a corrected GOM*/GEM slope of -0.88 (Figure 5, gray line). The corrected slope is close to -1 and therefore suggests that all nearly GOM produced has been retained within the free tropospheric air masses observed during the high GOM-event at the PDM.

$\delta^{202}Hg_{GEM}$ and $\Delta^{204}Hg_{GEM}$ during the high-GOM event were slightly but significantly higher, and $\Delta^{199}Hg_{GEM}$, $\Delta^{200}Hg_{GEM}$ and $\Delta^{201}Hg_{GEM}$ slightly but significantly lower than pre- and post-event samples during 20 - 28 Dec 2012 (Figure 1; t-test all $p<0.05$). All five GEM isotope signatures are significantly correlated with GEM (Figure

6) and GOM concentration. Net GEM oxidation therefore seems to have caused significant MDF, odd-MIF and even-MIF. The above analysis of the GOM event at the PDM suggests that the observed air masses represent the reactants, products and isotope fractionation characteristics of net GEM oxidation. Because the GOM-event was long-lived, displaying elevated GOM levels over 48 hours, we suggest that the GEM and GOM concentration, and GEM isotope observations represent a snapshot of net GEM oxidation that has been little influenced by further mixing with boundary layer air. This implies that the observed MDF, odd-MIF and even-MIF has accompanied net GEM oxidation in the lower troposphere. Previous observations on even-MIF in precipitation (Δ^{200}Hg only; Δ^{204}Hg not observed; Chen et al. 2012) led to the suggestion that even-MIF originates at the tropopause or stratosphere. Our results suggest that the even-MIF mechanism also operates within the free troposphere.

In Figure 6 we plot the GEM and RM (~GOM) isotope observations in Rayleigh diagrams, and fit MDF, odd-MIF and even-MIF factors for net GEM oxidation. Assuming pre-/post GOM event isotope observations as the starting point for GEM reactant in the free troposphere, we applied Rayleigh distillation equations for residual $\delta^{202}Hg_{GEM}$, $\Delta^{199}Hg_{GEM}$, $\Delta^{200}Hg_{GEM}$, $\Delta^{201}Hg_{GEM}$, and $\Delta^{204}Hg_{GEM}$ and for cumulative product GOM to estimate corresponding isotope fractionation factors $\varepsilon^{202/198}_{MDF(GOM-GEM)}$ of -1.1±0.2‰, $\varepsilon^{199/198}_{MIF(GOM-GEM)}$ of 0.65±0.11‰, $\varepsilon^{200/198}_{MIF(GOM-GEM)}$ of 0.22±0.05‰, $\varepsilon^{201/198}_{MIF(GOM-GEM)}$ of 0.65±0.10‰, and $\varepsilon^{204/198}_{MIF(GOM-GEM)}$ of -0.39±0.12‰ for the net GEM to GOM conversion observed (Figure 6). It should be kept in mind that these fractionation factor do not inform on whether oxidation or reduction is the underlying cause, i.e. they represent net oxidation.

Atmospheric GEM and RM pool size

GEM and RM represent the two dominant reduced and oxidized atmospheric Hg pools. The relative size of these two pools is not very well constrained due to limited mountain-top and in-flight measurements and bias in denuder based RM measurements (Jaffe et al., 2014). Recent global Hg chemistry and transport models indicate that RM (500 Mg) represents 12% and GEM 88% (3600 Mg) of atmospheric Hg, most of this residing in the free troposphere (Horowitz et al., 2017). Based on the newly observed free tropospheric RM and GEM isotope compositions (this study), and previously observed rainfall Hg, and modeled Hg emission fluxes and isotopic composition, we can estimate by isotopic mass balance the proportions of RM and GEM (Table 1). The Δ^{200}Hg signature, is best suited for this, since it is not confounded by additional even-MIF in cloud water, ocean or soil environment. Annual mean GEM Δ^{200}Hg at the PDM of -0.03±0.03‰ (Fu et al., 2016b) is identical to

GEM Δ^{200}Hg of -0.04‰ of the pre-/post GOM intrusion air masses, representing the northern hemisphere free tropospheric GEM pool. RM Δ^{200}Hg at PDM (0.15‰) is similar to mean northern hemispheric rainfall Δ^{200}Hg (0.13±0.06‰), suggesting that both values represent the free tropospheric RM pool. We use a model estimate for Δ^{200}Hg (0.02±0.02‰) of global Hg emissions (Sun et al., 2019) to constrain the mass balance, and calculate that 30±17% (1σ) of free tropospheric Hg should be present as RM in order to explain the rainfall, RM and GEM Δ^{200}Hg observations. This would suggest that current RM observations and models underestimate the size of the atmospheric RM pool by a factor of two. Our assessment is potentially biased due to the lack of observations in the southern hemisphere.

Acknowledgements

This work was supported by research grants ERC-2010-StG-20091028, ERC-2015-PoC-665482 from the European Research Council and the H2020 ERA-PLANET (689443) iGOSP programme to JES. We acknowledge technical support from the UMS 831 Pic du Midi Observatory team. This observatory is part of the P2OA (http://p2oa.aero.obs-mip.fr). P2OA facilities and staff are funded and supported by the University Paul Sabatier Toulouse 3, France, and CNRS (Centre National de la Recherche Scientifique). XY thanks the Chinese Scholarship Council for his PhD fellowship.

Author contributions

J.E.S conceived the study. X.F, N.M., Y.X, M.J. and J.E.S performed field sampling. X.F, N.M., Y.X, M.J, LEHB, JC. and J.E.S performed laboratory measurements. F.G. managed ancillary data collection at the PDM. X.F and J.E.S wrote the draft manuscript, which was improved by contributions from all authors.

Additional information

All Hg stable isotope data measured and discussed in this study is reported in the Supplementary Data.

References

Amos, H. M., Jacob, D. J., Holmes, C. D., Fisher, J. A., Wang, Q., Yantosca, R. M., Corbitt, E. S., Galarneau, E., Rutter, A. P., Gustin, M. S., Steffen, A., Schauer, J. J., Graydon, J. A., St Louis, V. L., Talbot, R. W., Edgerton, E. S., Zhang, Y. and Sunderland, E. M.: Gas-particle partitioning of atmospheric Hg(II) and its effect on global mercury deposition, Atmospheric Chemistry and Physics, 12(1), 591–603, doi:10.5194/acp-12-591-2012, 2012.

Ariya, P. A., Amyot, M., Dastoor, A., Deeds, D., Feinberg, A., Kos, G., Poulain, A., Ryjkov, A., Semeniuk, K., Subir, M. and Toyota, K.: Mercury Physicochemical and Biogeochemical Transformation in the Atmosphere and at Atmospheric Interfaces: A Review and Future Directions, Chemical Reviews, 115(10), 3760–3802, doi:10.1021/cr500667e, 2015.

Bagnato, E., Tamburello, G., Avard, G., Martinez-Cruz, M., Enrico, M., Fu, X., Sprovieri, M. and Sonke, J. E.: Mercury fluxes from volcanic and geothermal sources: an update., Geological Society, London, Special Publications, doi 10.1144/SP410.2, 2014.

Berg, T., Pfaffhuber, K. A., Cole, A. S., Engelsen, O. and Steffen, A.: Ten-year trends in atmospheric mercury concentrations, meteorological effects and climate variables at Zeppelin, Ny-Ålesund, Atmospheric Chemistry and Physics, 13(13), 6575–6586, doi:10.5194/acp-13-6575-2013, 2013.

Bergquist, B. A. and Blum, J. D.: Mass-Dependent and -Independent Fractionation of Hg Isotopes by Photoreduction in Aquatic Systems., Science, 318, 417–420, 2007.

Blum, J. D. and Bergquist, B. A.: Reporting of variations in the natural isotopic composition of mercury., Analytical and Bioanalytical Chemistry, 388, 353–359, 2007.

Blum, J. D., Sherman, L. S. and Johnson, M. W.: Mercury Isotopes in Earth and Environmental Sciences, in Annual Review of Earth and Planetary Sciences, Vol 42, vol. 42, edited by R. Jeanloz, pp. 249–269., 2014.

Buchachenko, A. L., Ivanov, V. L., Roznyatovskii, V. A., Artamkina, G. A., Vorob'ev, A. K. and Ustynyuk, Y. A.: Magnetic isotope effect for mercury nuclei in photolysis of Bis(p-trifluoromethylbenzyl)mercury., Doklady Physical Chemistry, 413, 39–41, 2007.

Chen, J., Hintelmann, H., Feng, X. and Dimock, B.: Unusual fractionation of both odd and even mercury isotopes in precipitation from Peterborough, ON, Canada, Geochimica et Cosmochimica Acta, 90, 33–46, doi:10.1016/j.gca.2012.05.005, 2012.

Demers, J. D., Blum, J. D. and Zak, D. R.: Mercury isotopes in a forested ecosystem: Implications for air-surface exchange dynamics and the global mercury cycle, Global Biogeochemical Cycles, 27(1), 222–238, doi:10.1002/gbc.20021, 2013.

Demoz, B., Collett, J., J. L. and Daube, J., B. C.: On the Caltech Active Strand Cloudwater Collectors., Atmospheric Research, 41, 47–62, 1996.

Dibble, T. S., Tetu, H. L., Jiao, Y., Thackray, C. P. and Jacob, D. J.: Modeling the OH-Initiated Oxidation of Mercury in the Global Atmosphere without Violating Physical Laws, Journal of Physical Chemistry A, 124(2), 444–453, doi:10.1021/acs.jpca.9b10121, 2020.

Donohoue, D. L., Bauer, D., Cossairt, B. and Hynes, A.: Temperature and pressure dependent rate coefficients for the reaction of Hg with Br and the reaction of Br with Br: A pulsed laser photolysis-pulsed laser induced fluorescence study, Journal of Physical Chemistry A, 110, 6623–6632, 2006.

Enrico, M., Le Roux, G., Marusczak, N., Heimbürger, L.-E., Claustres, A., Fu, X., Sun, R. and Sonke, J. E.: Atmospheric mercury transfer to peat bogs dominated by gaseous elemental mercury dry deposition., Environmental Science & Technology, doi:10.1021/acs.est.5b06058, 2016.

Fitzgerald, W. F. and Lamborg, C. H.: Geochemistry of Mercury in the Environment, in Treatise on Geochemistry, vol. 9, edited by E. D. Holland and K. K. Turekian, pp. 107–148, Elsevier-Pergamon, Oxford., 2004.

Fu, X., Heimburger, L. E. and Sonke, J. E.: Collection of atmospheric gaseous mercury for stable isotope analysis using iodine- and chlorine-impregnated activated carbon traps, Journal of Analytical Atomic Spectrometry, DOI: 10.1039/C3JA50356A, 2014.

Fu, X. W., Marusczak, N., Heimbürger, L. E., Sauvage, B., Gheusi, F. and Sonke, J. E.: Atmospheric mercury speciation dynamics at the high-altitude Pic du Midi Observatory, southern France, Atmospheric Chemistry and Physics, 16, 5623–5639, doi:10.5194/acp-16-5623-2016, 2016a.

Fu, X. W., Marusczak, N., Wang, X., Gheusi, F. and Sonke, J. E.: The isotopic composition of total gaseous mercury in the free troposphere of the Pic du Midi Observatory (2877 m a.s.l, France), Environmental Science & Technology, submitted, 2016b.

Gheusi, F., Ravetta, F., Delbarre, H., Tsamalis, C., Chevalier-Rosso, A., Leroy, C., Augustin, P., Delmas, R., Ancellet, G., Athier, G., Bouchou, P., Campistron, B., Cousin, J. M., Fourmentin, M. and Meyerfeld, Y.: Pic 2005, a field campaign to investigate low-tropospheric ozone variability in the Pyrenees, Atmospheric Research, 101(3), 640–665, doi:10.1016/j.atmosres.2011.04.014, 2011.

Gratz, L., Keeler, G., Blum, J. and Sherman, L. S.: Isotopic composition and fractionation of mercury in Great Lakes precipitation and ambient air, Environmental Science and Technology, 44, 7764–7770, 2010.

Gratz, L. E., Ambrose, J. L., Jaffe, D. A., Shah, V., Jaegle, L., Stutz, J., Festa, J., Spolaor, M., Tsai, C., Selin, N. E., Song, S., Zhou, X., Weinheimer, A. J., Knapp, D. J., Montzka, D. D., Flocke, F. M., Campos, T. L., Apel, E., Hornbrook, R., Blake, N. J., Hall, S., Tyndall, G. S., Reeves, M., Stechman, D. and Stell, M.: Oxidation of mercury by bromine in the subtropical Pacific free troposphere, Geophysical Research Letters, 42(23), doi:10.1002/2015gl066645, 2015.

Grissom, C. B.: Magnetic field effects in biology: A survey of possible mechanisms with emphasis on radical-pair recombination, Chemical Reviews, 95, 3–24, 1995.

Holmes, C. D., Jacob, D. J., Corbitt, E. S., Mao, J., Yang, X., Talbot, R. and Slemr, F.: Global atmospheric model for mercury including oxidation by bromine atoms, Atmospheric Chemistry and Physics, 10, 12037–12057, 2010.

Horowitz, H. M., Jacob, D. J., Zhang, Y., Dibble, T. S., Slemr, F., Amos, H. M., Schmidt, J. A., Corbitt, E. S., Marais, E. A. and Sunderland, E. M.: A new mechanism for atmospheric mercury redox chemistry: implications for the global mercury budget, Atmospheric Chemistry and Physics, 17(10), 6353–6371, doi:10.5194/acp-17-6353-2017, 2017.

Hulin, M., Gheusi, F., Lothon, M., Pont, V., Lohou, F., Ramonet, M., Delmotte, M., Derrien, S., Athier, G., Meyerfeld, Y., Bezombes, Y., Augustin, P. and Ravetta, F.: Observations of Thermally Driven Circulations in the Pyrenees: Comparison of Detection Methods and Impact on Atmospheric Composition Measured at a Mountaintop, Journal of Applied Meteorology and Climatology, 58(4), 717–740, doi:10.1175/JAMC-D-17-0268.1, 2019.

Jaffe, D. A., Lyman, S., Amos, H. M., Gustin, M. S., Huang, J., Selin, N. E., Levin, L., ter Schure, A., Mason, R. P., Talbot, R., Rutter, A., Finley, B., Jaegle, L., Shah, V., McClure, C., Arnbrose, J., Gratz, L., Lindberg, S., Weiss-Penzias, P., Sheu, G.-R., Feddersen, D., Horvat, M., Dastoor, A., Hynes, A. J., Mao, H., Sonke, J. E., Slemr, F., Fisher, J. A., Ebinghaus, R., Zhang, Y. and Edwards, G.: Progress on Understanding Atmospheric Mercury Hampered by Uncertain Measurements, Environmental Science & Technology, 48(13), 7204–7206, doi:10.1021/es5026432, 2014.

Jiskra, M., Wiederhold, J. G., Skyllberg, U., Kronberg, R.-M., Hajdas, I. and Kretzschmar, R.: Mercury Deposition and Re-emission Pathways in Boreal Forest Soils Investigated with Hg Isotope Signatures, Environmental Science & Technology, 49(12), 7188–7196, doi:10.1021/acs.est.5b00742, 2015.

Jiskra, M., Sonke, J. E., Agnan, Y., Helmig, D. and Obrist, D.: Insights from mercury stable isotopes on terrestrial-atmosphere exchange of Hg(0) in the Arctic tundra, Biogeosciences, 16(20), 4051–4064, doi:10.5194/bg-16-4051-2019, 2019.

Kritee, K., Blum, J. D., Reinfelder, J. R. and Barkay, T.: Microbial stable isotope fractionation of mercury: A synthesis of present understanding and future directions, Chemical Geology, this issue, doi:10.1016/j.chemgeo.2012.08.017, 2012.

Kwon, S. Y., Blum, J. D., Yin, R., Tsui, M. T.-K., Yang, Y. H. and Choi, J. W.: Mercury stable isotopes for monitoring the effectiveness of the Minamata Convention on Mercury, Earth-Science Reviews, 203, 103111, doi:https://doi.org/10.1016/j.earscirev.2020.103111, 2020.

Lyman, S. N. and Jaffe, D. A.: Formation and fate of oxidized mercury in the upper troposphere and lower stratosphere, Nature Geoscience, 5(2), 114–117, doi:10.1038/ngeo1353, 2011.

Lynam, M. M. and Keeler, G. J.: Comparison of methods for particulate phase mercury analysis: sampling and analysis, Analytical and Bioanalytical Chemistry, 374(6), 1009–1014, doi:10.1007/s00216-002-1584-4, 2002.

Marusczak, N., Sonke, J. E., Fu, X. and Jiskra, M.: Tropospheric GOM at the Pic du Midi Observatory-Correcting Bias in Denuder Based Observations, Environmental Science & Technology, 51(2), 863–869, doi:10.1021/acs.est.6b04999, 2017.

Motta, L. C., Blum, J. D., Johnson, M. W., Umhau, B. P., Popp, B. N., Washburn, S. J., Drazen, J. C., Benitez-Nelson, C. R., Hannides, C. C. S., Close, H. G. and Lamborg, C. H.: Mercury Cycling in the North Pacific Subtropical Gyre as Revealed by Mercury Stable Isotope Ratios, Global Biogeochemical Cycles, 33(6), 777–794, doi:10.1029/2018GB006057, 2019.

Motta, L. C., Kritee, K., Blum, J. D., Tsz-Ki Tsui, M. and Reinfelder, J. R.: Mercury Isotope Fractionation during the Photochemical Reduction of Hg(II) Coordinated with Organic Ligands., The journal of physical chemistry. A, doi:10.1021/acs.jpca.9b06308, 2020a.

Motta, L. C., Chien, A. D., Rask, A. E. and Zimmerman, P. M.: Mercury Magnetic Isotope Effect: A Plausible

Photochemical Mechanism, J. Phys. Chem. A, 124(19), 3711–3719, doi:10.1021/acs.jpca.0c00661, 2020b.

Obrist, D., Agnan, Y., Jiskra, M., Olson, C. L., Colegrove, D. P., Hueber, J., Moore, C. W., Sonke, J. E. and Helmig, D.: Tundra uptake of atmospheric elemental mercury drives Arctic mercury pollution, Nature, 547(7662), 201-+, doi:10.1038/nature22997, 2017.

Saiz-Lopez, A., Sitkiewicz, S. P., Roca-Sanjuán, D., Oliva-Enrich, J. M., Dávalos, J. Z., Notario, R., Jiskra, M., Xu, Y., Wang, F., Thackray, C. P., Sunderland, E. M., Jacob, D. J., Travnikov, O., Cuevas, C. A., Acuña, A. U., Rivero, D., Plane, J. M. C., Kinnison, D. E. and Sonke, J. E.: Photoreduction of gaseous oxidized mercury changes global atmospheric mercury speciation, transport and deposition, Nature Communications, 9(1), 4796, doi:10.1038/s41467-018-07075-3, 2018.

Saiz-Lopez, A., Acuña, A. U., Trabelsi, T., Carmona-García, J., Dávalos, J. Z., Rivero, D., Cuevas, C. A., Kinnison, D. E., Sitkiewicz, S. P., Roca-Sanjuán, D. and Francisco, J. S.: Gas-Phase Photolysis of Hg(I) Radical Species: A New Atmospheric Mercury Reduction Process, J. Am. Chem. Soc., 141(22), 8698–8702, doi:10.1021/jacs.9b02890, 2019.

Schauble, E. A.: Role of nuclear volume in driving equilibrium isotope fractionation of mercury, thallium, and other very heavy elements., Geochimica et Cosmochimca Acta, 71, 2170–2189, 2007.

Seigneur, C. and Lohman, K.: Effect of bromine chemistry on the atmospheric mercury cycle, Journal of Geophysical Research - Atmosphere, 113, D23309, 2008.

Seigneur, C., Vijayaraghavan, K., Lohman, K., Karamchandani, P. and Scott, C.: Global Source Attribution for Mercury Deposition in the United States, Environmental Science and Technology, 38, 555–569, 2004.

Shah, V., Jaegle, L., Gratz, L. E., Ambrose, J. L., Jaffe, D. A., Selin, N. E., Song, S., Campos, T. L., Flocke, F. M., Reeves, M., Stechman, D., Stell, M., Festa, J., Stutz, J., Weinheimer, A. J., Knapp, D. J., Montzka, D. D., Tyndall, G. S., Apel, E. C., Hornbrook, R. S., Hills, A. J., Riemer, D. D., Blake, N. J., Cantrell, C. A. and Mauldin, R. L.: Origin of oxidized mercury in the summertime free troposphere over the southeastern US, Atmospheric Chemistry and Physics, 16(3), 1511–1530, doi:10.5194/acp-16-1511-2016, 2016.

Sherman, L. S., Blum, J. D., Keeler, G. J., Demers, J. D. and Dvonch, J. T.: Investigation of Local Mercury Deposition from a Coal-Fired Power Plant Using Mercury Isotopes, Environmental Science & Technology, 46(1), 382–390, doi:10.1021/es202793c, 2012.

Steffen, A., Schroeder, W., Macdonald, R., Poissant, L. and Konoplev, A.: Mercury in the Arctic atmosphere: An analysis of eight years of measurements of GEM at Alert (Canada) and a comparison with observations at Amderma (Russia) and Kuujjuarapik (Canada), Science of the Total Environment, 342(1–3), 185–198, doi:10.1016/j.scitotenv.2004.12.048, 2005.

Streets, D. G., Horowitz, H. M., Lu, Z., Levin, L., Thackray, C. P. and Sunderland, E. M.: Global and regional trends in mercury emissions and concentrations, 2010-2015, Atmospheric Environment, 201, 417–427, doi:10.1016/j.atmosenv.2018.12.031, 2019.

Sun, G., Sommar, J., Feng, X., Lin, C.-J., Ge, M., Wang, W., Yin, R., Fu, X. and Shang, L.: Mass-Dependent and -Independent Fractionation of Mercury Isotope during Gas-Phase Oxidation of Elemental Mercury Vapor by Atomic

Cl and Br, Environ. Sci. Technol., 50(17), 9232–9241, doi:10.1021/acs.est.6b01668, 2016.

Sun, R., Enrico, M., Heimbürger, L.-E., Scott, C. and Sonke, J. E.: A double-stage tube furnace-acid-trapping protocol for the pre-concentration of mercury from solid samples for isotopic analysis, Analytical and Bioanalytical Chemistry, 405(21), 6771–6781, doi:10.1007/s00216-013-7152-2, 2013.

Sun, R., Jiskra, M., Amos, H. M., Zhang, Y., Sunderland, E. M. and Sonke, J. E.: Modelling the mercury stable isotope distribution of Earth surface reservoirs: Implications for global Hg cycling, Geochimica et Cosmochimica Acta, 246, 156–173, doi:https://doi.org/10.1016/j.gca.2018.11.036, 2019.

Swartzendruber, P. C., Jaffe, J. A., Prestbo, E. M., Weiss-Penzias, P., Selin, N. E., Park, R., Jacob, D. J., Strode, S. and Jaegle, L.: Observations of reactive gaseous mercury in the free troposphere at the Mount Bachelor Observatory, Journal of Geophysical Research, 111, D24301, 2006.

Timonen, H., Ambrose, J. L. and Jaffe, D. A.: Oxidation of elemental Hg in anthropogenic and marine airmasses, Atmospheric Chemistry and Physics, 13(5), 2827–2836, doi:10.5194/acp-13-2827-2013, 2013.

Turro, N. J.: Influence of nuclear spin on chemical, reactions: Magnetic isotope and.magnetic field effects (A Review), Proceedings of the National Academy of Science USA, 80, 609–621, 1983.

Wang, F., Saiz-Lopez, A., Mahajan, A. S., Gomez Martin, J. C., Armstrong, D., Lemes, M., Hay, T. and Prados-Roman, C.: Enhanced production of oxidised mercury over the tropical Pacific Ocean: a key missing oxidation pathway, Atmospheric Chemistry and Physics, 14(3), 1323–1335, doi:10.5194/acp-14-1323-2014, 2014.

Wang, Z., Chen, J., Feng, X., Hintelmann, H., Yuan, S., Cai, H., Huang, Q., Wang, S. and Wang, F.: Mass-dependent and mass-independent fractionation of mercury isotopes in precipitation from Guiyang, SW China, Comptes Rendus Geoscience, 347(7), 358–367, doi:https://doi.org/10.1016/j.crte.2015.02.006, 2015.

Weiss-Penzias, P., Amos, H. M., Selin, N. E., Gustin, M. S., Jaffe, D. A., Obrist, D., Sheu, G. R. and Giang, A.: Use of a global model to understand speciated atmospheric mercury observations at five high-elevation sites, Atmospheric Chemistry and Physics, 15(3), 1161–1173, doi:10.5194/acp-15-1161-2015, 2015.

Wiederhold, J. G., Cramer, C. J., Daniel, K., Infante, I., Bourdon, B. and Kretzschmar, R.: Equilibrium mercury isotope fractionation between dissolved Hg(II) species and thiol-bound Hg, Environmental Science and Technology, 44, 4191–4197, 2010.

Yang, X., Jiskra, M. and Sonke, J. E.: Experimental rainwater divalent mercury speciation and photoreduction rates in the presence of halides and organic carbon, Science of The Total Environment, 697, 133821, doi:https://doi.org/10.1016/j.scitotenv.2019.133821, 2019.

Zheng, W. and Hintelmann, H.: Mercury isotope fractionation during photoreduction in natural water is controlled by its Hg/DOC ratio., Geochimica et Cosmochimca Acta, 73, 6704–6715, 2009.

Zheng, W. and Hintelmann, H.: Isotope Fractionation of Mercury during Its Photochemical Reduction by Low-Molecular-Weight Organic Compounds, Journal of Physical Chemistry A, 114, 4246–4253, 2010.

Ariya, P. A., Amyot, M., Dastoor, A., Deeds, D., Feinberg, A., Kos, G., Poulain, A., Ryjkov, A., Semeniuk, K., Subir, M. and Toyota, K.: Mercury Physicochemical and Biogeochemical Transformation in the Atmosphere and at Atmospheric Interfaces: A Review and Future Directions, Chemical Reviews, 115(10), 3760–3802, doi:10.1021/cr500667e, 2015.

Bagnato, E., Tamburello, G., Avard, G., Martinez-Cruz, M., Enrico, M., Fu, X., Sprovieri, M. and Sonke, J. E.: Mercury fluxes from volcanic and geothermal sources: an update., Geological Society, London, Special Publications, doi 10.1144/SP410.2, 2014.

Berg, T., Pfaffhuber, K. A., Cole, A. S., Engelsen, O. and Steffen, A.: Ten-year trends in atmospheric mercury concentrations, meteorological effects and climate variables at Zeppelin, Ny-Ålesund, Atmospheric Chemistry and Physics, 13(13), 6575–6586, doi:10.5194/acp-13-6575-2013, 2013.

Bergquist, B. A. and Blum, J. D.: Mass-Dependent and -Independent Fractionation of Hg Isotopes by Photoreduction in Aquatic Systems., Science, 318, 417–420, 2007.

Blum, J. D. and Bergquist, B. A.: Reporting of variations in the natural isotopic composition of mercury., Analytical and Bioanalytical Chemistry, 388, 353–359, 2007.

Blum, J. D., Sherman, L. S. and Johnson, M. W.: Mercury Isotopes in Earth and Environmental Sciences, in Annual Review of Earth and Planetary Sciences, Vol 42, vol. 42, edited by R. Jeanloz, pp. 249–269., 2014.

Buchachenko, A. L., Ivanov, V. L., Roznyatovskii, V. A., Artamkina, G. A., Vorob'ev, A. K. and Ustynyuk, Y. A.: Magnetic isotope effect for mercury nuclei in photolysis of Bis(p-trifluoromethylbenzyl)mercury., Doklady Physical Chemistry, 413, 39–41, 2007.

Chen, J., Hintelmann, H., Feng, X. and Dimock, B.: Unusual fractionation of both odd and even mercury isotopes in precipitation from Peterborough, ON, Canada, Geochimica et Cosmochimica Acta, 90, 33–46, doi:10.1016/j.gca.2012.05.005, 2012.

Demers, J. D., Blum, J. D. and Zak, D. R.: Mercury isotopes in a forested ecosystem: Implications for air-surface exchange dynamics and the global mercury cycle, Global Biogeochemical Cycles, 27(1), 222–238, doi:10.1002/gbc.20021, 2013.

Demoz, B., Collett, J., J. L. and Daube, J., B. C.: On the Caltech Active Strand Cloudwater Collectors., Atmospheric Research, 41, 47–62, 1996.

Dibble, T. S., Tetu, H. L., Jiao, Y., Thackray, C. P. and Jacob, D. J.: Modeling the OH-Initiated Oxidation of Mercury in the Global Atmosphere without Violating Physical Laws, Journal of Physical Chemistry A, 124(2), 444–453, doi:10.1021/acs.jpca.9b10121, 2020.

Donohoue, D. L., Bauer, D., Cossairt, B. and Hynes, A.: Temperature and pressure dependent rate coefficients for the reaction of Hg with Br and the reaction of Br with Br: A pulsed laser photolysis-pulsed laser induced fluorescence study, Journal of Physical Chemistry A, 110, 6623–6632, 2006.

Enrico, M., Le Roux, G., Marusczak, N., Heimbürger, L.-E., Claustres, A., Fu, X., Sun, R. and Sonke, J. E.: Atmospheric mercury transfer to peat bogs dominated by gaseous elemental mercury dry deposition., Environmental

Science & Technology, doi:10.1021/acs.est.5b06058, 2016.

Fitzgerald, W. F. and Lamborg, C. H.: Geochemistry of Mercury in the Environment, in Treatise on Geochemistry, vol. 9, edited by E. D. Holland and K. K. Turekian, pp. 107–148, Elsevier-Pergamon, Oxford., 2004.

Fu, X., Heimburger, L. E. and Sonke, J. E.: Collection of atmospheric gaseous mercury for stable isotope analysis using iodine- and chlorine-impregnated activated carbon traps, Journal of Analytical Atomic Spectrometry, DOI: 10.1039/C3JA50356A, 2014.

Fu, X. W., Marusczak, N., Heimbürger, L. E., Sauvage, B., Gheusi, F. and Sonke, J. E.: Atmospheric mercury speciation dynamics at the high-altitude Pic du Midi Observatory, southern France, Atmospheric Chemistry and Physics, 16, 5623–5639, doi:10.5194/acp-16-5623-2016, 2016a.

Fu, X. W., Marusczak, N., Wang, X., Gheusi, F. and Sonke, J. E.: The isotopic composition of total gaseous mercury in the free troposphere of the Pic du Midi Observatory (2877 m a.s.l, France), Environmental Science & Technology, submitted, 2016b.

Gheusi, F., Ravetta, F., Delbarre, H., Tsamalis, C., Chevalier-Rosso, A., Leroy, C., Augustin, P., Delmas, R., Ancellet, G., Athier, G., Bouchou, P., Campistron, B., Cousin, J. M., Fourmentin, M. and Meyerfeld, Y.: Pic 2005, a field campaign to investigate low-tropospheric ozone variability in the Pyrenees, Atmospheric Research, 101(3), 640–665, doi:10.1016/j.atmosres.2011.04.014, 2011.

Gratz, L., Keeler, G., Blum, J. and Sherman, L. S.: Isotopic composition and fractionation of mercury in Great Lakes precipitation and ambient air, Environmental Science and Technology, 44, 7764–7770, 2010.

Gratz, L. E., Ambrose, J. L., Jaffe, D. A., Shah, V., Jaegle, L., Stutz, J., Festa, J., Spolaor, M., Tsai, C., Selin, N. E., Song, S., Zhou, X., Weinheimer, A. J., Knapp, D. J., Montzka, D. D., Flocke, F. M., Campos, T. L., Apel, E., Hornbrook, R., Blake, N. J., Hall, S., Tyndall, G. S., Reeves, M., Stechman, D. and Stell, M.: Oxidation of mercury by bromine in the subtropical Pacific free troposphere, Geophysical Research Letters, 42(23), doi:10.1002/2015gl066645, 2015.

Grissom, C. B.: Magnetic field effects in biology: A survey of possible mechanisms with emphasis on radical-pair recombination, Chemical Reviews, 95, 3–24, 1995.

Holmes, C. D., Jacob, D. J., Corbitt, E. S., Mao, J., Yang, X., Talbot, R. and Slemr, F.: Global atmospheric model for mercury including oxidation by bromine atoms, Atmospheric Chemistry and Physics, 10, 12037–12057, 2010.

Horowitz, H. M., Jacob, D. J., Zhang, Y., Dibble, T. S., Slemr, F., Amos, H. M., Schmidt, J. A., Corbitt, E. S., Marais, E. A. and Sunderland, E. M.: A new mechanism for atmospheric mercury redox chemistry: implications for the global mercury budget, Atmospheric Chemistry and Physics, 17(10), 6353–6371, doi:10.5194/acp-17-6353-2017, 2017.

Hulin, M., Gheusi, F., Lothon, M., Pont, V., Lohou, F., Ramonet, M., Delmotte, M., Derrien, S., Athier, G., Meyerfeld, Y. : Observations of plain-mountain circulation in the Pyrenees : detection methods and impact on atmospheric composition measured at a mountain top, J. Applied. Meteor. Climatol, 2019, 58, 717–740, https://doi.org/10.1175/JAMC-D-17-0268.1.

Jaffe, D. A., Lyman, S., Amos, H. M., Gustin, M. S., Huang, J., Selin, N. E., Levin, L., ter Schure, A., Mason, R. P.,

Talbot, R., Rutter, A., Finley, B., Jaegle, L., Shah, V., McClure, C., Arnbrose, J., Gratz, L., Lindberg, S., Weiss-Penzias, P., Sheu, G.-R., Feddersen, D., Horvat, M., Dastoor, A., Hynes, A. J., Mao, H., Sonke, J. E., Slemr, F., Fisher, J. A., Ebinghaus, R., Zhang, Y. and Edwards, G.: Progress on Understanding Atmospheric Mercury Hampered by Uncertain Measurements, Environmental Science & Technology, 48(13), 7204–7206, doi:10.1021/es5026432, 2014.

Jiskra, M., Wiederhold, J. G., Skyllberg, U., Kronberg, R.-M., Hajdas, I. and Kretzschmar, R.: Mercury Deposition and Re-emission Pathways in Boreal Forest Soils Investigated with Hg Isotope Signatures, Environmental Science & Technology, 49(12), 7188–7196, doi:10.1021/acs.est.5b00742, 2015.

Jiskra, M., Sonke, J. E., Agnan, Y., Helmig, D. and Obrist, D.: Insights from mercury stable isotopes on terrestrial-atmosphere exchange of Hg(0) in the Arctic tundra, Biogeosciences, 16(20), 4051–4064, doi:10.5194/bg-16-4051-2019, 2019.

Kritee, K., Blum, J. D., Reinfelder, J. R. and Barkay, T.: Microbial stable isotope fractionation of mercury: A synthesis of present understanding and future directions, Chemical Geology, this issue, doi:10.1016/j.chemgeo.2012.08.017, 2012.

Kwon, S. Y., Blum, J. D., Yin, R., Tsui, M. T.-K., Yang, Y. H. and Choi, J. W.: Mercury stable isotopes for monitoring the effectiveness of the Minamata Convention on Mercury, Earth-Science Reviews, 203, 103111, doi:https://doi.org/10.1016/j.earscirev.2020.103111, 2020.

Lyman, S. N. and Jaffe, D. A.: Formation and fate of oxidized mercury in the upper troposphere and lower stratosphere, Nature Geoscience, 5(2), 114–117, doi:10.1038/ngeo1353, 2011.

Lynam, M. M. and Keeler, G. J.: Comparison of methods for particulate phase mercury analysis: sampling and analysis, Analytical and Bioanalytical Chemistry, 374(6), 1009–1014, doi:10.1007/s00216-002-1584-4, 2002.

Marusczak, N., Sonke, J. E., Fu, X. and Jiskra, M.: Tropospheric GOM at the Pic du Midi Observatory-Correcting Bias in Denuder Based Observations, Environmental Science & Technology, 51(2), 863–869, doi:10.1021/acs.est.6b04999, 2017.

Motta, L. C., Blum, J. D., Johnson, M. W., Umhau, B. P., Popp, B. N., Washburn, S. J., Drazen, J. C., Benitez-Nelson, C. R., Hannides, C. C. S., Close, H. G. and Lamborg, C. H.: Mercury Cycling in the North Pacific Subtropical Gyre as Revealed by Mercury Stable Isotope Ratios, Global Biogeochemical Cycles, 33(6), 777–794, doi:10.1029/2018GB006057, 2019.

Motta, L. C., Kritee, K., Blum, J. D., Tsz-Ki Tsui, M. and Reinfelder, J. R.: Mercury Isotope Fractionation during the Photochemical Reduction of Hg(II) Coordinated with Organic Ligands., The journal of physical chemistry. A, doi:10.1021/acs.jpca.9b06308, 2020a.

Motta, L. C., Chien, A. D., Rask, A. E. and Zimmerman, P. M.: Mercury Magnetic Isotope Effect: A Plausible Photochemical Mechanism, J. Phys. Chem. A, 124(19), 3711–3719, doi:10.1021/acs.jpca.0c00661, 2020b.

Obrist, D., Agnan, Y., Jiskra, M., Olson, C. L., Colegrove, D. P., Hueber, J., Moore, C. W., Sonke, J. E. and Helmig, D.: Tundra uptake of atmospheric elemental mercury drives Arctic mercury pollution, Nature, 547(7662), 201-+, doi:10.1038/nature22997, 2017.

Saiz-Lopez, A., Sitkiewicz, S. P., Roca-Sanjuán, D., Oliva-Enrich, J. M., Dávalos, J. Z., Notario, R., Jiskra, M., Xu, Y., Wang, F., Thackray, C. P., Sunderland, E. M., Jacob, D. J., Travnikov, O., Cuevas, C. A., Acuña, A. U., Rivero, D., Plane, J. M. C., Kinnison, D. E. and Sonke, J. E.: Photoreduction of gaseous oxidized mercury changes global atmospheric mercury speciation, transport and deposition, Nature Communications, 9(1), 4796, doi:10.1038/s41467-018-07075-3, 2018.

Saiz-Lopez, A., Acuña, A. U., Trabelsi, T., Carmona-García, J., Dávalos, J. Z., Rivero, D., Cuevas, C. A., Kinnison, D. E., Sitkiewicz, S. P., Roca-Sanjuán, D. and Francisco, J. S.: Gas-Phase Photolysis of Hg(I) Radical Species: A New Atmospheric Mercury Reduction Process, J. Am. Chem. Soc., 141(22), 8698–8702, doi:10.1021/jacs.9b02890, 2019.

Schauble, E. A.: Role of nuclear volume in driving equilibrium isotope fractionation of mercury, thallium, and other very heavy elements., Geochimica et Cosmochimca Acta, 71, 2170–2189, 2007.

Seigneur, C. and Lohman, K.: Effect of bromine chemistry on the atmospheric mercury cycle, Journal of Geophysical Research - Atmosphere, 113, D23309, 2008.

Seigneur, C., Vijayaraghavan, K., Lohman, K., Karamchandani, P. and Scott, C.: Global Source Attribution for Mercury Deposition in the United States, Environmental Science and Technology, 38, 555–569, 2004.

Shah, V., Jaegle, L., Gratz, L. E., Ambrose, J. L., Jaffe, D. A., Selin, N. E., Song, S., Campos, T. L., Flocke, F. M., Reeves, M., Stechman, D., Stell, M., Festa, J., Stutz, J., Weinheimer, A. J., Knapp, D. J., Montzka, D. D., Tyndall, G. S., Apel, E. C., Hornbrook, R. S., Hills, A. J., Riemer, D. D., Blake, N. J., Cantrell, C. A. and Mauldin, R. L.: Origin of oxidized mercury in the summertime free troposphere over the southeastern US, Atmospheric Chemistry and Physics, 16(3), 1511–1530, doi:10.5194/acp-16-1511-2016, 2016.

Sherman, L. S., Blum, J. D., Keeler, G. J., Demers, J. D. and Dvonch, J. T.: Investigation of Local Mercury Deposition from a Coal-Fired Power Plant Using Mercury Isotopes, Environmental Science & Technology, 46(1), 382–390, doi:10.1021/es202793c, 2012.

Steffen, A., Schroeder, W., Macdonald, R., Poissant, L. and Konoplev, A.: Mercury in the Arctic atmosphere: An analysis of eight years of measurements of GEM at Alert (Canada) and a comparison with observations at Amderma (Russia) and Kuujjuarapik (Canada), Science of the Total Environment, 342(1–3), 185–198, doi:10.1016/j.scitotenv.2004.12.048, 2005.

Streets, D. G., Horowitz, H. M., Lu, Z., Levin, L., Thackray, C. P. and Sunderland, E. M.: Global and regional trends in mercury emissions and concentrations, 2010-2015, Atmospheric Environment, 201, 417–427, doi:10.1016/j.atmosenv.2018.12.031, 2019.

Sun, G., Sommar, J., Feng, X., Lin, C.-J., Ge, M., Wang, W., Yin, R., Fu, X. and Shang, L.: Mass-Dependent and -Independent Fractionation of Mercury Isotope during Gas-Phase Oxidation of Elemental Mercury Vapor by Atomic Cl and Br, Environ. Sci. Technol., 50(17), 9232–9241, doi:10.1021/acs.est.6b01668, 2016.

Sun, R., Enrico, M., Heimbürger, L.-E., Scott, C. and Sonke, J. E.: A double-stage tube furnace-acid-trapping protocol for the pre-concentration of mercury from solid samples for isotopic analysis, Analytical and Bioanalytical Chemistry, 405(21), 6771–6781, doi:10.1007/s00216-013-7152-2, 2013.

Sun, R., Jiskra, M., Amos, H. M., Zhang, Y., Sunderland, E. M. and Sonke, J. E.: Modelling the mercury stable isotope distribution of Earth surface reservoirs: Implications for global Hg cycling, Geochimica et Cosmochimica Acta, 246, 156–173, doi:https://doi.org/10.1016/j.gca.2018.11.036, 2019.

Swartzendruber, P. C., Jaffe, J. A., Prestbo, E. M., Weiss-Penzias, P., Selin, N. E., Park, R., Jacob, D. J., Strode, S. and Jaegle, L.: Observations of reactive gaseous mercury in the free troposphere at the Mount Bachelor Observatory, Journal of Geophysical Research, 111, D24301, 2006.

Timonen, H., Ambrose, J. L. and Jaffe, D. A.: Oxidation of elemental Hg in anthropogenic and marine airmasses, Atmospheric Chemistry and Physics, 13(5), 2827–2836, doi:10.5194/acp-13-2827-2013, 2013.

Turro, N. J.: Influence of nuclear spin on chemical, reactions: Magnetic isotope and.magnetic field effects (A Review), Proceedings of the National Academy of Science USA, 80, 609–621, 1983.

Wang, F., Saiz-Lopez, A., Mahajan, A. S., Gomez Martin, J. C., Armstrong, D., Lemes, M., Hay, T. and Prados-Roman, C.: Enhanced production of oxidised mercury over the tropical Pacific Ocean: a key missing oxidation pathway, Atmospheric Chemistry and Physics, 14(3), 1323–1335, doi:10.5194/acp-14-1323-2014, 2014.

Wang, Z., Chen, J., Feng, X., Hintelmann, H., Yuan, S., Cai, H., Huang, Q., Wang, S. and Wang, F.: Mass-dependent and mass-independent fractionation of mercury isotopes in precipitation from Guiyang, SW China, Comptes Rendus Geoscience, 347(7), 358–367, doi:https://doi.org/10.1016/j.crte.2015.02.006, 2015.

Weiss-Penzias, P., Amos, H. M., Selin, N. E., Gustin, M. S., Jaffe, D. A., Obrist, D., Sheu, G. R. and Giang, A.: Use of a global model to understand speciated atmospheric mercury observations at five high-elevation sites, Atmospheric Chemistry and Physics, 15(3), 1161–1173, doi:10.5194/acp-15-1161-2015, 2015.

Wiederhold, J. G., Cramer, C. J., Daniel, K., Infante, I., Bourdon, B. and Kretzschmar, R.: Equilibrium mercury isotope fractionation between dissolved Hg(II) species and thiol-bound Hg, Environmental Science and Technology, 44, 4191–4197, 2010.

Yang, X., Jiskra, M. and Sonke, J. E.: Experimental rainwater divalent mercury speciation and photoreduction rates in the presence of halides and organic carbon, Science of The Total Environment, 697, 133821, doi:https://doi.org/10.1016/j.scitotenv.2019.133821, 2019.

Zheng, W. and Hintelmann, H.: Mercury isotope fractionation during photoreduction in natural water is controlled by its Hg/DOC ratio., Geochimica et Cosmochimca Acta, 73, 6704–6715, 2009.

Zheng, W. and Hintelmann, H.: Isotope Fractionation of Mercury during Its Photochemical Reduction by Low-Molecular-Weight Organic Compounds, Journal of Physical Chemistry A, 114, 4246–4253, 2010.

Table 1. Mean Δ^{200}Hg signatures for Hg emissions and atmospheric reservoirs. Mean and 1σ for published rainfall data represents the mean of means of remote site data points for each study in order to avoid site type and sample number bias. Global GEM emission Δ^{200}Hg was calculated from the listed Hg fluxes and modeled Δ^{200}Hg. The combined uncertainty on calculated atmospheric GEM and RM fractions was propagated from uncertainties on observational data for emissions and RM and GEM Δ^{200}Hg.

Sample type	**Hg flux**	**Δ^{200}Hg**	**1σ**	
	Mg y^{-1}	‰	‰	
Pic du Midi RM		0.15	0.12	This study
Rainfall Hg		0.13	0.06	(Blum et al., 2014; Demers et al., 2013; Enrico et al., 2016; Gratz et al., 2010; Motta et al., 2019; Obrist et al., 2017; Sherman et al., 2012; Wang et al., 2015)
Pic du Midi GEM		-0.03	0.02	This study, (Fu et al., 2016b)
Ocean GEM emission	4600	0.03		(Horowitz et al., 2017; Sun et al., 2019)
Anthropogenic GEM	1470	0		(Horowitz et al., 2017; Sun et al., 2019)
Soil GEM emission	1420	-0.02		(Horowitz et al., 2017; Sun et al., 2019)
Volcanic GEM emission	250	0		(Horowitz et al., 2017; Sun et al., 2019)
Global GEM emission	7740	0.02	0.02	(Horowitz et al., 2017; Sun et al., 2019)
f(RM)		0.30[a]	0.17	
f(GEM)		0.70[a]	0.17	

[a] calculated from mass balance: Δ^{200}Hg(global GEM emitted) = f(RM) × Δ^{200}Hg(rainfall) + f(GEM) × Δ^{200}Hg(PDM GEM), and f(RM) + f(GEM) = 1

Figure 1. Hg speciation and isotope variability during a free tropospheric air mass intrusion. From 20 to 28 Dec 2012, high frequency (12h, 24h) gaseous elemental Hg^0 (GEM) isotope signatures $\delta^{202}Hg$, $\Delta^{199}Hg$, $\Delta^{200}Hg$ (A), CO and O_3 concentrations (B), atmospheric GOM, PBM and GEM concentrations (C), and solar radiation and relative air humidity (D) showed a 48h long intrusion of a free tropospheric air mass, high in GOM, and low in GEM and humidity.

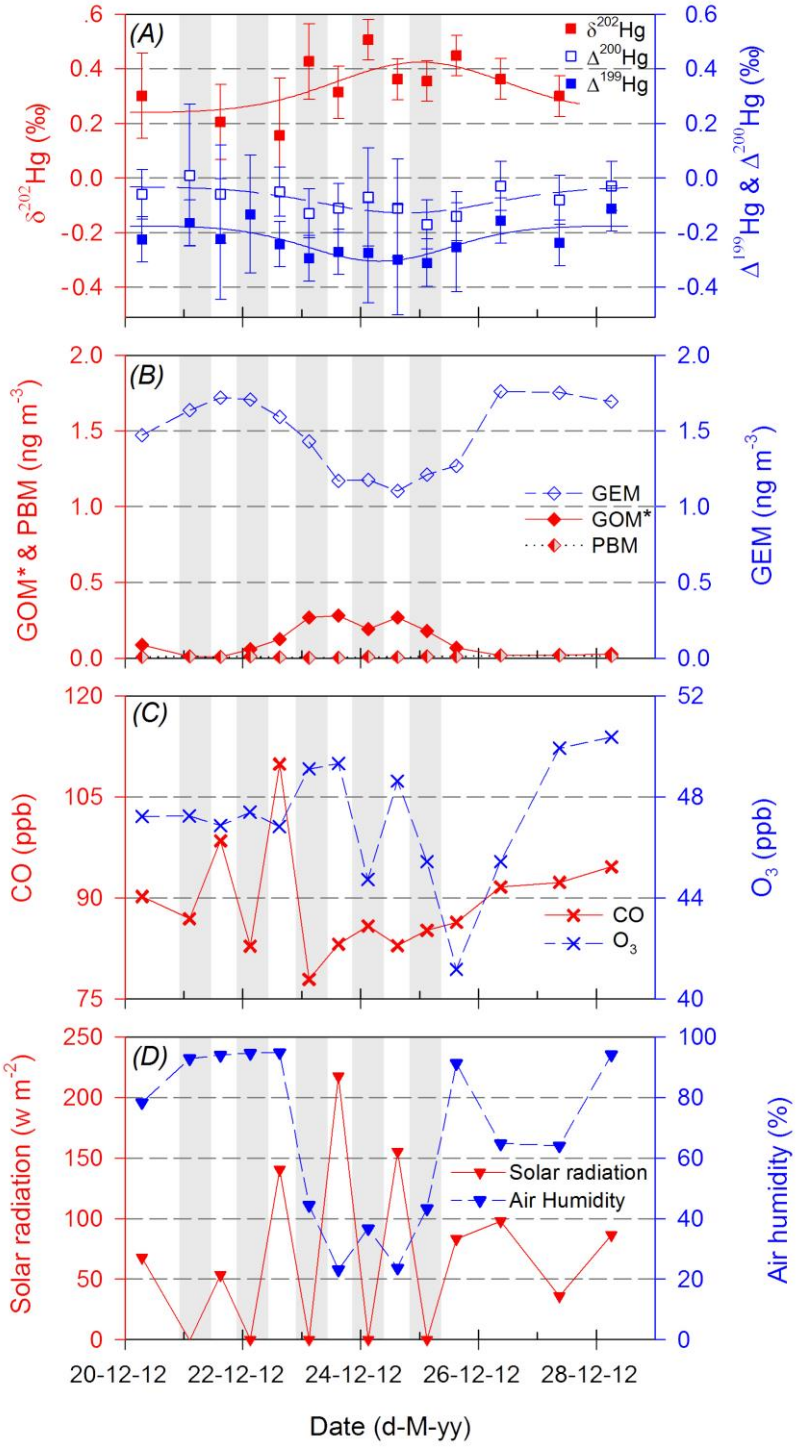

Figure 2. Air mass back-trajectories of the free tropospheric air mass intrusion. 7-day backward trajectories of the high frequency (12h, 24h) gaseous elemental Hg^0 (GEM) isotope samples obtained from 20 to 28 Dec 2012: Travelling height (A, indicated by air pressure), air mass humidity (B), solar radiation (C), and air temperature (D). Date and time labels are mid-points of 12h and 24h Hg isotope sampling windows.

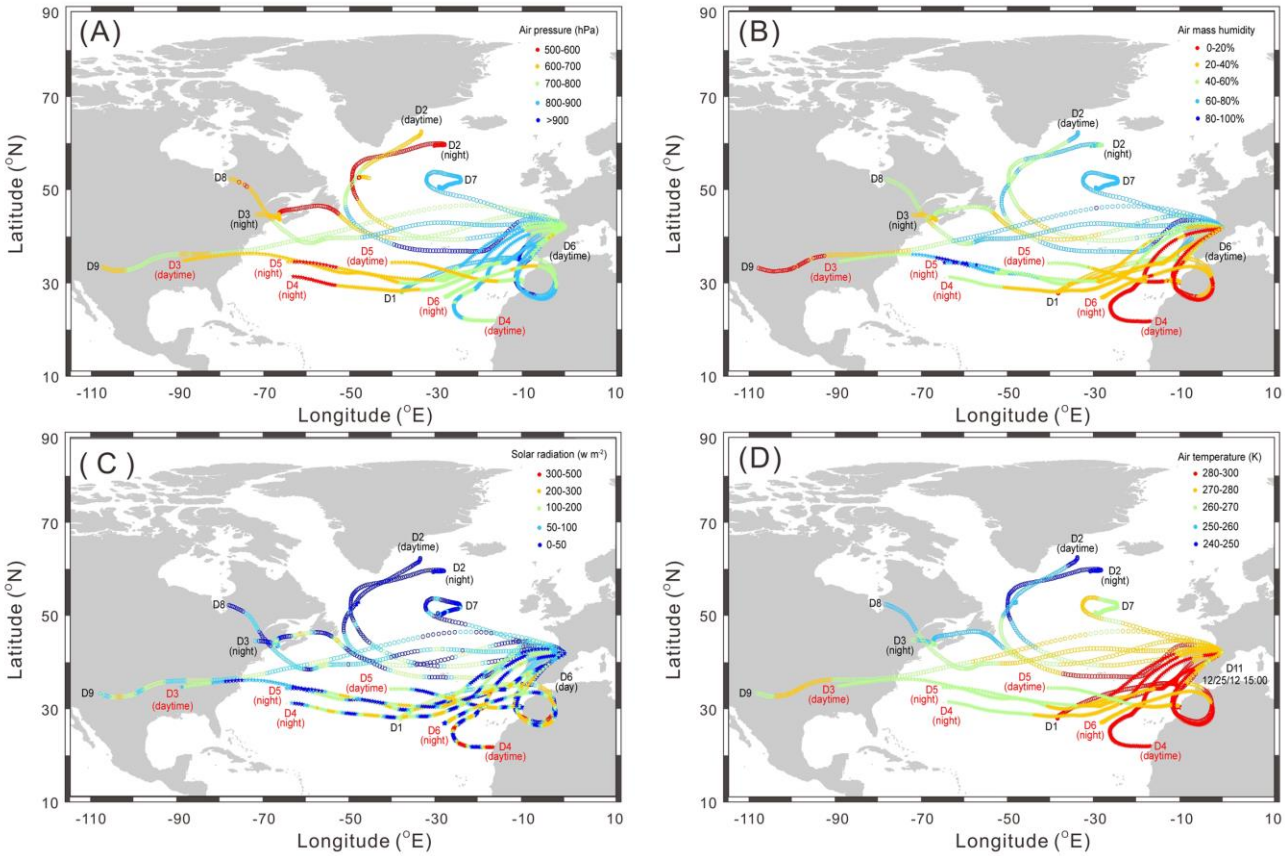

Figure 3. Atmospheric Hg stable isotope variation at the Pic du Midi. Hg mass dependent (δ^{202}Hg) and mass independent (Δ^{199}Hg, Δ^{200}Hg, Δ^{201}Hg, Δ^{204}Hg) isotope signatures in reactive Hg (RM=GOM+PBM), cloud water, 12h/24h GEM from this study, and previously published GEM (Fu et al., 2014) and rainfall (Enrico et al., 2016).

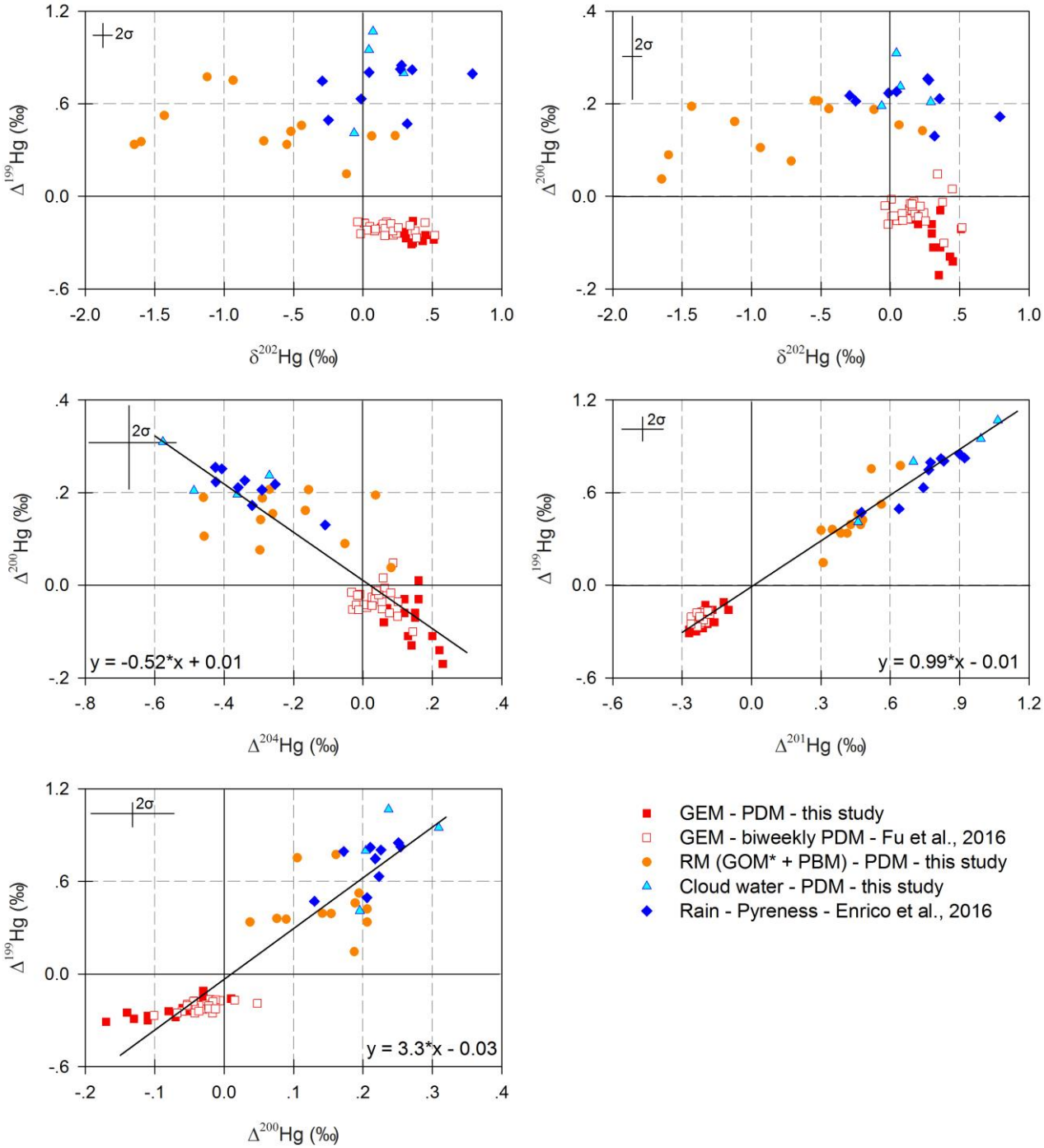

Figure 4. Δ^{196}Hg measurement of rainfall. A 20.5L rainfall sample containing 6.0 ng L^{-1} of Hg was pre-concentrated 1200x to deliver a 0.015V signal on ^{196}Hg. The resulting Δ^{196}Hg signature is -0.06 ± 0.19‰ (2σ, n=2) suggesting that nuclear self-shielding is not the underlying cause of atmospheric even-Hg MIF. A Δ^{202}Hg of 0 is indicated in the graph, since the Δ^{xxx}Hg (where xxx are Hg isotopes masses 196 to 204) are calculated relative to $\delta^{202/198}$Hg ratios, themselves anchored to the ^{198}Hg reference isotope.

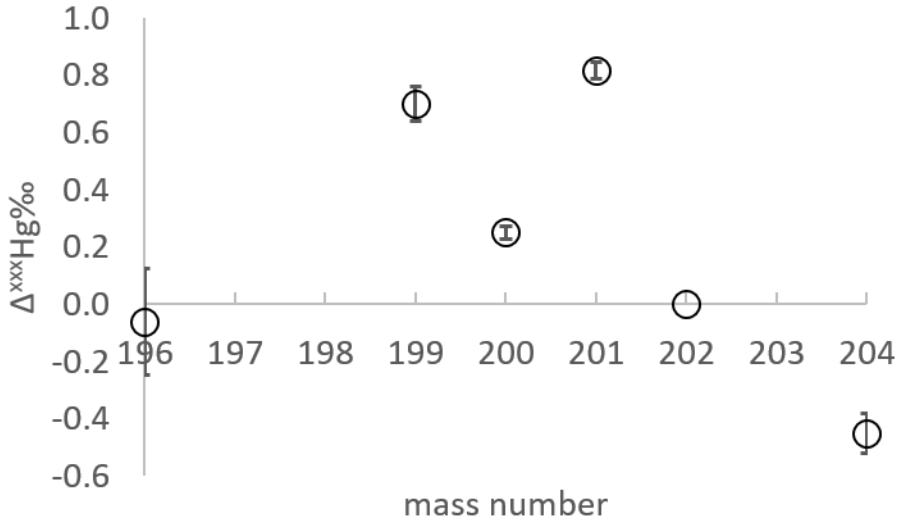

Figure 5. Hg oxidation mass balance in free tropospheric air at the Pic du Midi. Relationship between gaseous elemental Hg^0 (GEM, ng m^{-3}) and gaseous oxidized Hg^{II} (GOM*, ng m^{-3}) observed during the nine day sampling campaign at PDM. Black circles and grey diamonds are Tekran GEM and GOM* data (Extended Data), where grey diamonds represent the high GOM event only. A slope of -1 is indicative of Hg mass conservation during GEM oxidation to GOM in the observed air mass. The uncorrected GOM*/GEM slope of -0.44 is biased low due to latitudinal bias in the GEM precursor to GOM (see main text). Latitude corrected subtropical Atlantic Ocean GEM levels (grey square) indicate a slope of -0.88, suggesting that Hg mass has been conserved in the high GOM air mass detected at PDM.

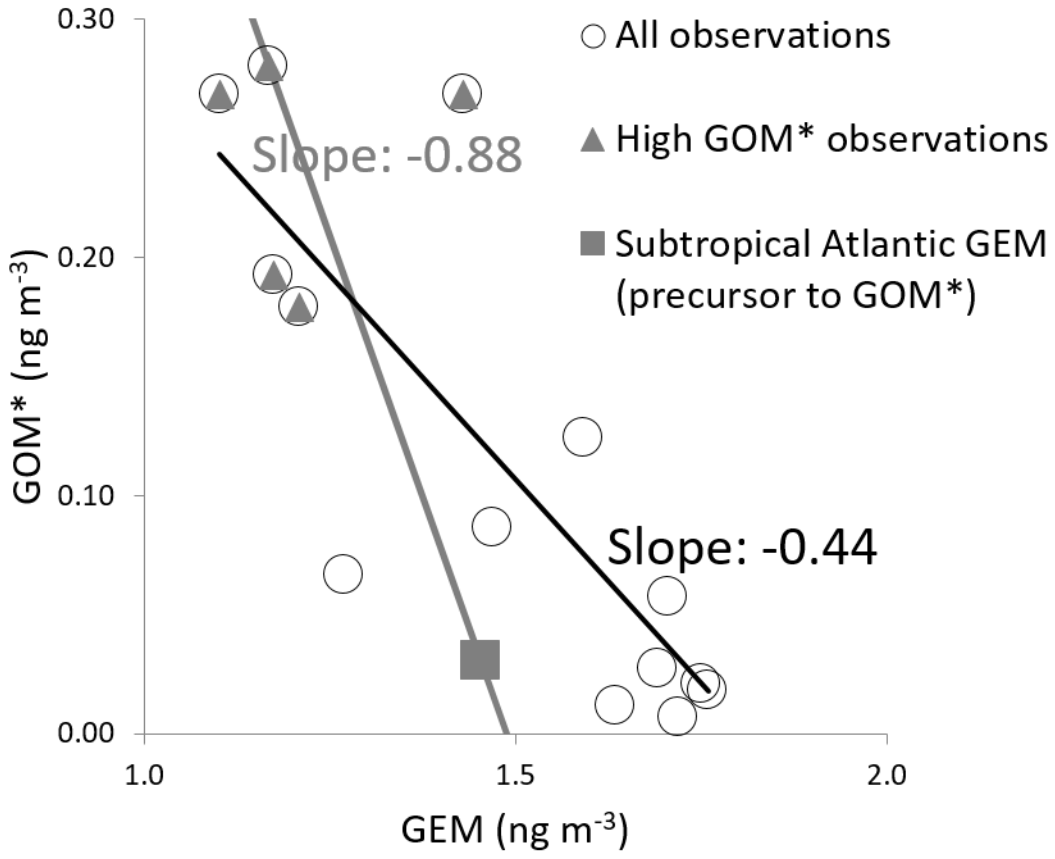

Figure 6. Rayleigh diagrams for Hg isotope fractionation during Hg^0 net oxidation. This dataset is a composite of GEM isotope composition (red diamonds) recorded in the Atlantic Ocean free tropospheric air mass intrusion at PDM in Dec 2012, and mean RM (=GOM*+PBM ~ GOM*) isotope composition (blue triangles) at PDM recorded from June – October 2014. Isotope fractionation factors $\varepsilon^{\delta 202}_{MDF(GOM-GEM)}$ of -1.1 ± 0.2‰, $\varepsilon^{\Delta 199}_{MIF(GOM-GEM)}$ of 0.65 ± 0.11‰, $\varepsilon^{\Delta 200}_{MIF(GOM-GEM)}$ of 0.22 ± 0.05‰, $\varepsilon^{\Delta 201}_{MIF(GOM-GEM)}$ of 0.65 ± 0.10‰, and $\varepsilon^{\Delta 204}_{MIF(GOM-GEM)}$ of -0.39 ± 0.12‰ (all 1SE) were fitted by log-linear regression of Rayleigh equations for residual GEM and cumulative GOM*. All 12h and 24h observations (blue diamonds) over the nine day period were included in the fitting. The starting isotopic composition (green square) is the mean annual GEM composition at PDM (Fu et al., 2016b).

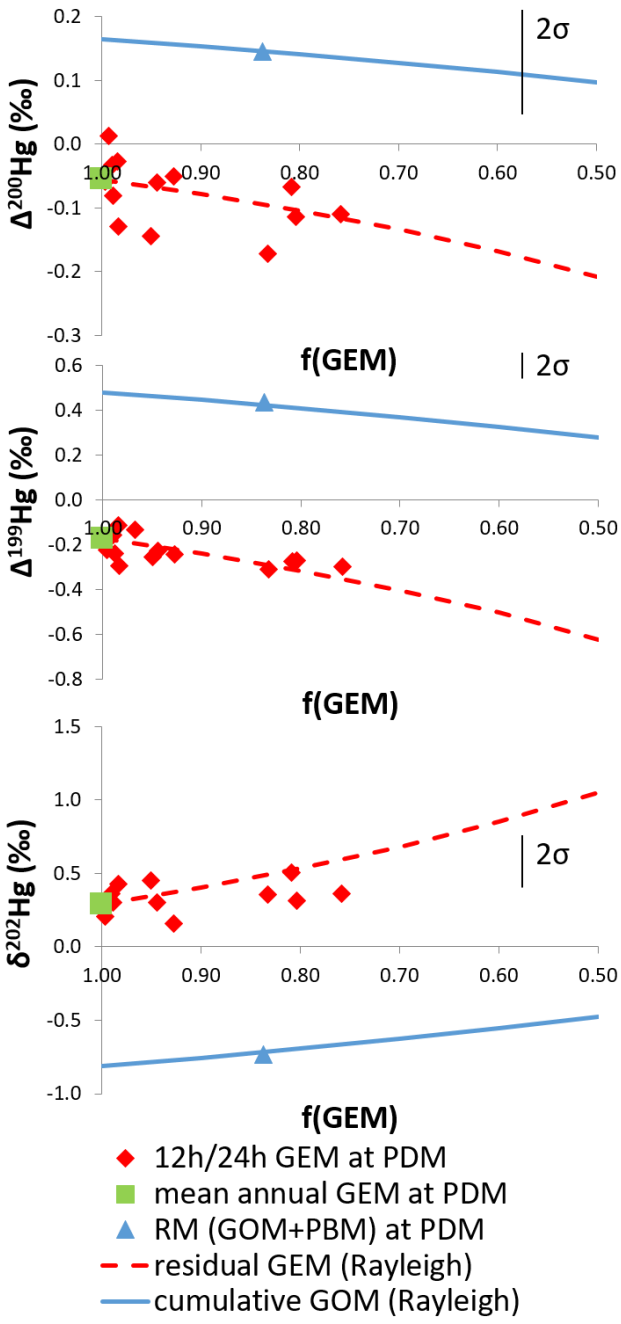
0.2
0.1
0.0
-0.1
-0.2
-0.3
Δ200Hg (‰)
2σ
1.00
0.90
0.80
0.70
0.60
0.50
f(GEM)
0.6
0.4
0.2
0.0
-0.2
-0.4
-0.6
-0.8
Δ199Hg (‰)
2σ
f(GEM)
1.5
1.0
0.5
0.0
-0.5
-1.0
δ202Hg (‰)
2σ
f(GEM)
12h/24h GEM at PDM
mean annual GEM at PDM
RM (GOM+PBM) at PDM
residual GEM (Rayleigh)
cumulative GOM (Rayleigh)

725
726